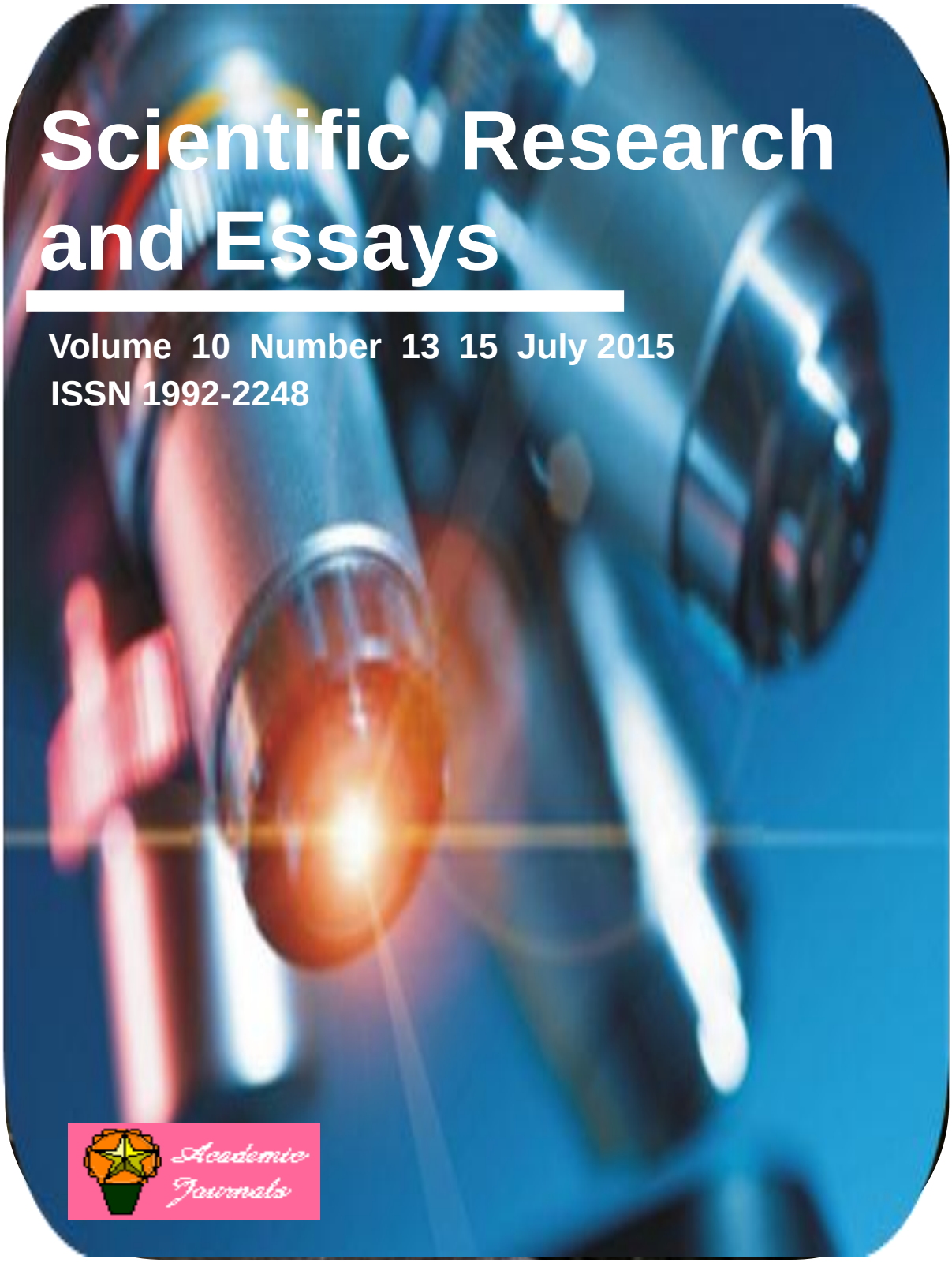

Scientific Research and Essays

Volume 10 Number 13 15 July 2015
ISSN 1992-2248

Academic Journals

ABOUTSRE

The**ScientificResearchandEssays(SRE)**ispublishedtwice monthly(onevolumeperyear)byAcademicJournals.

Scientific Research andEssays(SRE)isanopen accessjournal withtheobjectiveofpublishingqualityresearcharticlesinscience,medicine,agricultureandengineeringsuchasNanotechnology,ClimateChangeandGlobalWarming,AirPollutionManagementandElectronicsetc.AllpaperspublishedbySREareblindpeerreviewed.

SubmissionofManuscript

Submitmanuscriptsasemail attachment totheEditorialOfficeatsre@academicjournals.org.Amanuscriptnumberwillbemailedtothecorrespondingauthorshortlyaftersubmission.

TheScientificResearchandEssayswillonlyacceptmanuscriptssubmittedase-mailattachments.

Pleasereadthe**InstructionsforAuthors**beforesubmittingyourmanuscript.Themanuscriptfilesshouldbegiventhelastnameofthefirstauthor.

Editors

EditorialBoard

ScientificResearchandEssays

Table of Contents: Volume 10 Number 13 15 July, 2015

ARTICLES

Research Articles

academicJournals

Vol. 10(13), pp. 421-429, 15 July, 2015
DOI: 10.5897/SRE2015.6267
Article Number:4BFBF9A54031
ISSN 1992-2248

http://www.academicjournals.org/SRE

Scientific Research and Essays

Full Length Research Paper

Growth, optical, thermal and electrical properties of nonlinear optical γ-glycine single crystal

N. Nithya[1]*, R. Mahalakshmi[2] and S. Sagadevan[3]

[1]Department of Physics, Sree Sastha College of Engineering, Chembarambakkam, Chennai, 600 123, India.
[2]Department of Physics, GKM College of Engineering and Technology, Chennai-600 063, India.
[3]Department of Physics, Sree Sastha Institute of Engineering and Technology, Chennai-600 123, India.

Received 28 May, 2015; Accepted 24 June, 2015

Single crystal growth of γ-glycine has been grown by solution growth technique. The lattice parameters and crystal system of the grown crystals were confirmed by single crystal X-ray diffraction analysis. The functional groups present in the grown crystal were identified by FT-IR spectral analysis. The optical property of the γ-glycine crystal is studied by UV-Visible spectrum. Optical constants such as band gap, refractive index, extinction coefficient and electrical susceptibility were calculated to analyze the optical property from UV-Visible spectrum. The thermal analyses revealed good thermal stability of the material thus proving its suitability for NLO applications. The second harmonic generation (SHG) test has been confirmed by the Kurtz powder test. The dielectric studies of γ-glycine crystal were studied in the different frequency and different temperatures. Photoconductivity measurements were carried out in order to reveal the negative photoconductivity of the γ-glycine crystal.

Key words: Nonlinear optical (NLO), single x-ray diffraction, UV-visible spectrum, second-harmonic generation (SHG), dielectric constant, dielectric loss.

INTRODUCTION

Single crystal growth has a prominent role in the present era of rapid scientific and technical advancement, whereas the application of crystals has unbounded limits. Single crystal may be briefed out as the ordered array of atoms in repeated groups that shows characteristic symmetry elements by which the entire block of the material is built. Lots of basic science focuses the property of the crystal which depends on the production of high quality crystals with reasonable size. Nonlinear optical (NLO) materials have come upon the materials science scene and are being studied by many research groups around the world. These materials operate on light in a way very analogous to the way of semiconductors which operate on electrons to produce very fast electronic switching and computing circuits. Amino acids have proton donor carboxylic acid (COO^-) groups and proton acceptor amino (NH_2) groups. The importance of amino acids in NLO applications is due to the fact that all amino acids have a chiral symmetry and crystallize in noncentro-symmetric space groups. Amino acids and their complexes belong to a family of organic materials that have NLO applications (Prasad and

*Corresponding author. E-mail: n.nithya2011@gmail.com

Williams, 1991; Chemla and Zyss, 1987; Sagadevan,2014; Sagadevan, 2014).

Aminoacid family crystals are gaining importance as highly feasible second order NLO materials. The α-aminoacid, glycine forms addition compounds with a number of inorganic materials, especially inorganic acids. Complexes of glycine with inorganic acid /salts are promising materials for optical second harmonic generation as they tend to combine advantages of the organic aminoacid with that of the inorganic salt. These materials exhibit promising structural background in view of their zwitterionic, protonated forms and structural stabilization with hydrogen bonding. These factors account for the delocalization and corresponding enhancement in second order NLO activity. The carboxylic acid group present in the γ-glycine donates its proton to the amino group to form a salt of structure $CH_3CH\ COO^-\ NH_3^+$. Thus in the solid state, γ-glycine exist as a dipolar ion in which carboxyl group is presented as carboxylate ion and amino group is presented as ammonium ion. Due to this dipolar nature, it has a high melting point. The growth mechanism of γ-glycine is not a standard one and it depends on parameters such as impurities, solvent and pH of the growth medium. The γ-glycine, because its non-centrosymmetry structure makes it a suitable candidate for piezoelectric and nonlinear optical applications. The present investigation deals with the growth of γ-glycine single crystal that was grown by slow evaporation technique. The grown crystals were characterized by single crystal X-ray analysis, FTIR, UV spectral analysis, thermal, dielectric, SHG, and photoconductivity measurements. The results of these studies have been discussed in this paper in detail.

Crystal growth of γ-glycine

Glycine (grade AR) and hydrogen fluoride (grade AR) were used as such without further purification. Glycine and hydrogen fluoride were mixed in an equimolar ratio (1:1). The solutions of glycine and hydrogen fluoride were mixed together and the resulting solution was stirred for 5 h, to get a homogenous mixture. The solution was filtered to remove the solid impurities in the mother solution using an ultrapore filter and kept undisturbed in room temperature. Due to slow evaporation of the solution, spontaneous nucleation occurs and these are grown into crystals of comparable size. The synthesized salt was then purified by repeated crystallization. Transparent colourless crystals were harvested in a period of 2 weeks. Figure 1 shows as-grown crystals of γ-glycine.

RESULTS AND DISCUSSION

Single-crystal x-ray diffraction

The single-crystal X-ray diffraction analysis of the grown crystals was carried out to identify the cell parameters. From the single crystal X-ray diffraction analysis, we found that the lattice parameters were calculated to be a = 7.023 Å, b = 7.024 Å, c = 5.412 Å. It exhibits hexagonal crystal system with the space group of $P3_1$.The ORTEP representation of the molecule with atom numbering scheme is shown in Figure 2 and the packing diagram is shown in Figure 3. From the structural point of view, in γ-glycine, the carboxylate oxygen is electrostatically bonded by the hydrogen atom of NH_3 and forms strong H-bond along the c-axis. The crystal structure packing diagram shows that there are three molecules present per unit cell.

FTIR spectral analysis

In order to analyze qualitatively, the presence of functional groups in γ-glycine, Fourier transform infrared (FTIR) spectrum was recorded in the range 450 and 4000 cm^{-1} using Bruker IFS 66V. The sample used was in pellet form embedded with KBr phase. The middle infrared FTIR spectrum of γ-glycine is shown in Figure 4. There is a broad envelope between 2200 and 3600 cm^{-1}, and this includes NH vibrations at 3113 cm^{-1}, CH vibrations at 2892 cm^{-1} and NH vibrations at 2602 cm^{-1}. The OH vibrations are not clearly seen and hence the amino acid is zwitterionic. The sharp peak at 2168 cm^{-1} is due to the asymmetrical NH bend and torsional oscillation of NH_3^+ is seen at 503 cm^{-1}. The peak at 1594 cm^{-1} is broad and it is due to COO^- stretch and asymmetric NH_3^+ bend is seen at 1488 cm^{-1}. The symmetrical COO^- stretch occurs at 1393 cm^{-1}. The peak at 1335 cm^{-1} is due to CH bend.

UV-Vis-NIR spectral analysis

The UV-Visible spectrum of γ-glycine single crystal was recorded in the wavelength region 200 to 1000 nm and it is shown in Figure 5. For optical fabrications, the crystal should be highly transparent in the considered region of wavelength (Suresh and Arivuoli, 2011; Koteeswari and Sagadevan, 2014). The favorable transmittance of the crystal in the entire visible region suggests its suitability for second harmonic generation (Suresh and Anand, 2012). The UV absorption edge for the grown crystal was observed to be around 315 nm. The dependence of optical absorption coefficient on photon energy helps to study the band structure and type of transition of electrons (Sagadevan, 2014) (Figure 6). There is no absorption of light to an appreciable extent in the visible range of the electromagnetic spectrum, which is the intrinsic property of all the amino acids. It should be pointed out that γ-glycine presents a good optical transparency at the wavelength of source commonly used in SHG devices such as Nd: YAG laser. The optical absorption coefficient (α) was calculated from

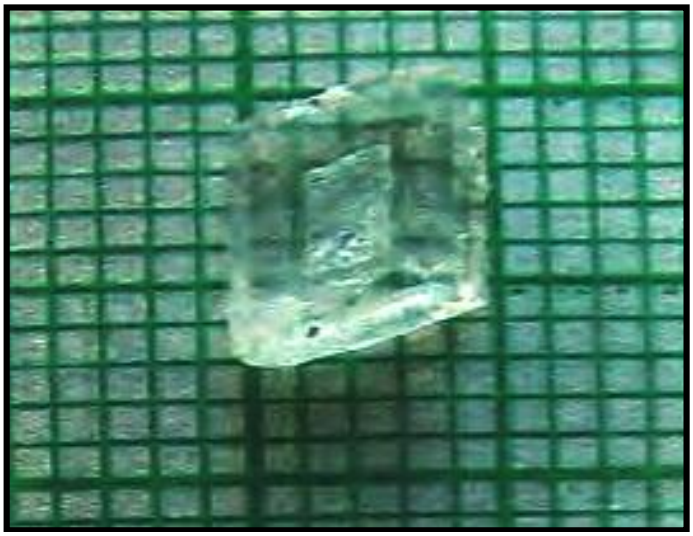

Figure 1. Photograph of grown γ-glycine single crystal.

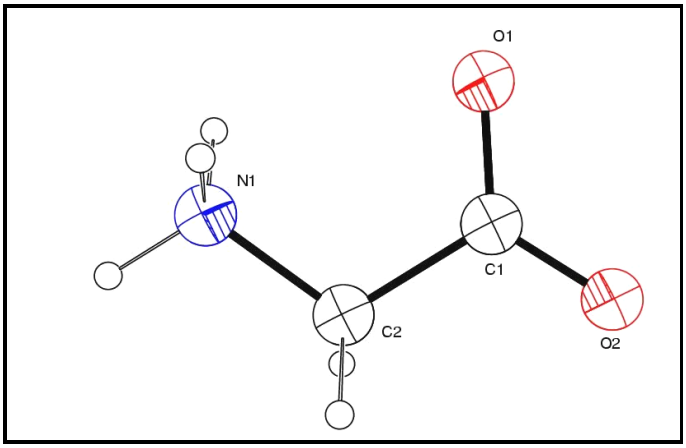

Figure 2. ORTEP representation of γ-glycine crystals.

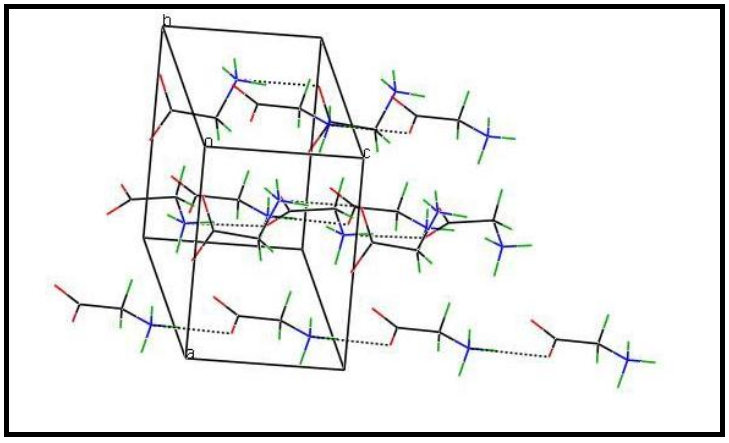

Figure 3. Packing of molecules in γ-glycine single crystal.

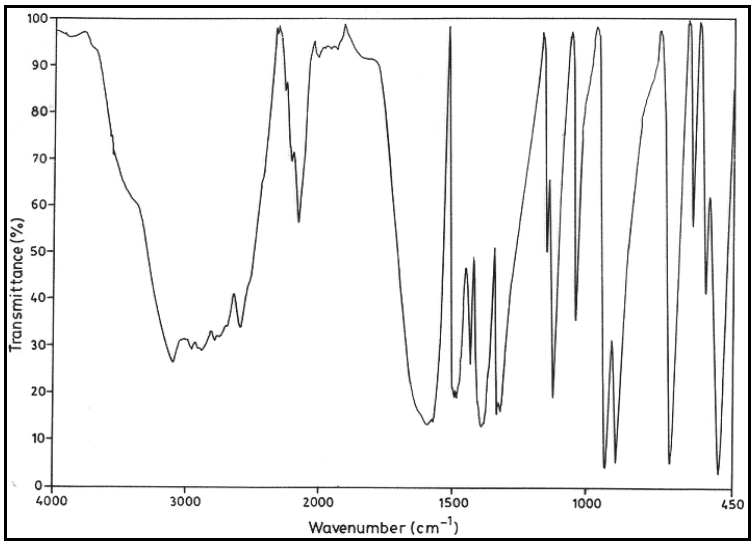

Figure 4. FTIR spectrum of γ-glycine single crystal.

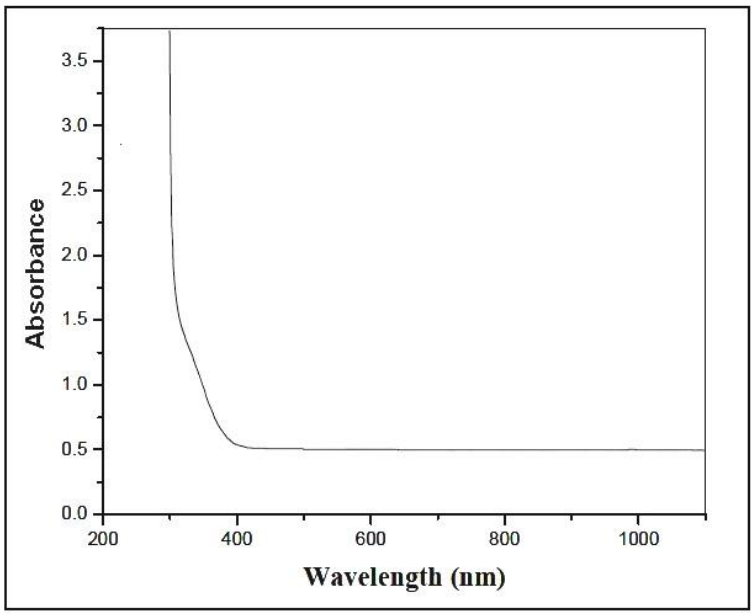

Figure 5. UV- Visible spectrum of γ-glycine crystal.

transmittance using the following relation:

$$\alpha = \frac{1}{d}\log\left(\frac{1}{T}\right) \quad (1)$$

Where *T* is the transmittance and *d* is the thickness of the crystal. As a direct band gap material, the crystal under study has an absorption coefficient (*α*) obeying the following relation for high photon energies (hv)

$$\alpha = \frac{A(h\nu - E_g)^{1/2}}{h\nu} \quad (2)$$

Where E_g is the optical band gap of the crystal and A is a constant. A plot of variation of $(\alpha h\nu)^2$ versus hv is shown in Fig.4. E_g is evaluated using the extrapolation of the linear part. Using Tauc's plot, the energy gap (E_g) was calculated as 3.7 eV and the large band gap clearly indicates the wide transparency of the crystal.

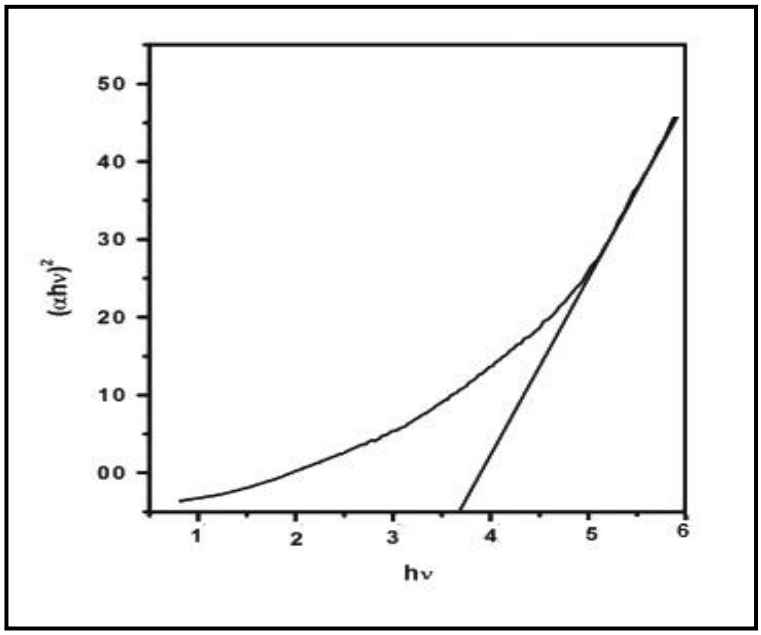

Figure 6. Plot of $(\alpha h\nu)^2$ vs photon energy.

This high band gap value indicates that the grown crystal possesses dielectric behaviour to induce polarization when powerful radiation is incident on the material.

Determination of optical constants

Two of the most important optical properties: the refractive index and the extinction coefficient which are generally called optical constants. The amount of light that transmits through material depends on the amount of the reflection and absorption that takes place along the light path. The optical constants such as the refractive index (n), the real dielectric constant (ε_r) and the imaginary part of dielectric constant (ε_i) were calculated using UV- Visible spectrum.The extinction coefficient (K) can be obtained from the following equation:

$$K = \frac{\lambda\alpha}{4\pi} \tag{3}$$

The extinction coefficient (K) was found to be 4.2 x 10^{-6} at λ = 1000 nm. The transmittance (T) is given by Sagadevan and Murugasen (2014):

$$T = \frac{(1-R)^2 \exp(-\alpha t)}{1-R^2 \exp(-2\alpha t)} \tag{4}$$

Reflectance (R) in terms of absorption coefficient can be obtained from the above equation. Hence:

$$R = \frac{1 \pm \sqrt{1-\exp(-\alpha t + \exp(\alpha t)}}{1+\exp(-\alpha t)} \tag{5}$$

Refractive index (n) can be determined from reflectance data using the following equation,

$$n = -\frac{(R+1) \pm \sqrt{3R^2+10R-3}}{2(R-1)} \tag{6}$$

The refractive index (n) was found to be 1.625 at λ = 1000 nm. From the optical constants, electric susceptibility (χ_c) can be calculated according to the following relation:

$$\varepsilon_r = \varepsilon_0 + 4\pi\chi_C = n^2 - k^2 \tag{7}$$

Hence,

$$\chi_C = \frac{n^2 - k^2 - \varepsilon_0}{4\pi} \tag{8}$$

where ε_0 is the permittivity of free space. The value of electric susceptibility χ_C is 0.152 at λ =1000 nm. The real part dielectric constant ε_r and imaginary part dielectric constant ε_i can be calculated from the

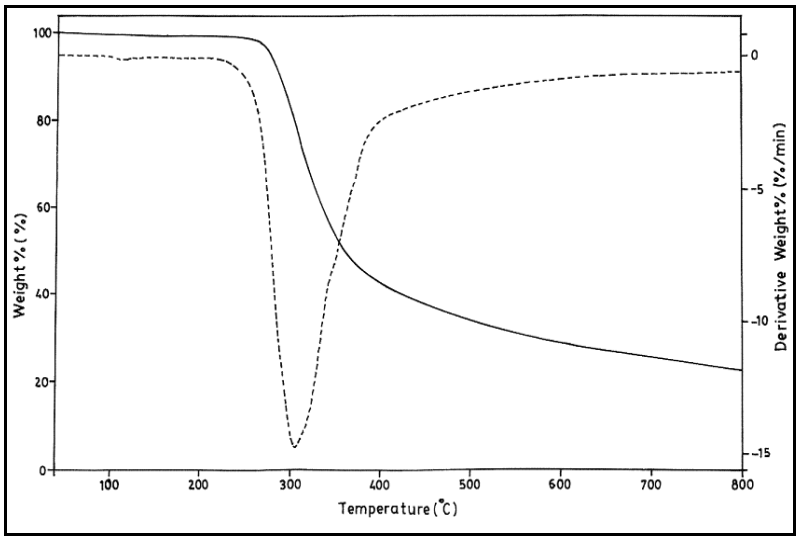

Figure 7. The TG-DTA curve of γ-glycine.

following relations:

$$\varepsilon_r = n^2 - k^2 \quad (9)$$

$$\varepsilon_i = 2nk \quad (10)$$

The value of real ε_r and ε_i imaginary dielectric constants at λ = 1000 nm were estimated as 1.752 and 6.302 x 10^{-5}, respectively. The lower value of dielectric constant and the positive value of the material are capable of producing induced polarization due to intense incident light radiation (Sagadevan and Murugasen, 2014).

NLO test – Kurtz powder SHG method

In this technique, the powdered sample with an average particle sizes range 125 to 150 μm is filled in a microcapillary tube about 1.5 mm diameter. Q-switched Nd: YAG laser emitting a fundamental wavelength of 1064 nm with an input power of 6.2 mJ/pulse and a pulse width of 8 ns with a repetition rate of 10 Hz was made to fall normally on the sample. The output from the sample was monochromated to collect the intensity of 532 nm component and to eliminate the fundamental wavelength. The second harmonic radiation generated by the randomly oriented micro crystals was focused by a lens and detected and a photo multiplier tube. The generation of the second harmonic was confirmed by a strong bright green emission emerging from the powdered sample. A potassium dihydrogen phosphate (KDP) crystal was used as a reference material in the SHG measurement. The results indicate that the efficiency is found to be 1.5 times greater than that of pure KDP.

Thermal analysis

The thermal analysis of γ-glycine crystal was carried out using Perkin Elmer thermal analyzer. The sample of weight 4.178 mg was taken in a crucible and subjected to a heating rate of 20°C per min in nitrogen atmosphere. The obtained thermo gram is shown in Figure 7. γ-glycine transforms irreversibly into α-glycine at a temperature of 168°C. The peak at 280°C is due to the decomposition of glycine. The thermo gram shows only one step of decomposition at 305°C, which is assigned to the melting point of the crystal. The single step decomposition at 303°C confirms the purity of the crystal without any incorporation of impurities and water of hydration in the lattice of the crystal. At 800°C about 78.398% of the sample decomposes leaving only 22.712% as an end residue. The DTA curve shows a sharp irreversible endothermic peak at 305°C which agree with the TG curve and confirms the melting point of the crystal. From the thermal analysis (TG-DTA), it is confirmed that the crystal is thermally stable up to 305°C without any thermal strain.

Dielectric studies

Dielectric properties are related with the electric field distribution within solid materials. γ-glycine crystals were selected and polished by soft polishing pad with fine grade alumina powder. The face of single crystal was cut in to rectangular shape and well-polished, so that it

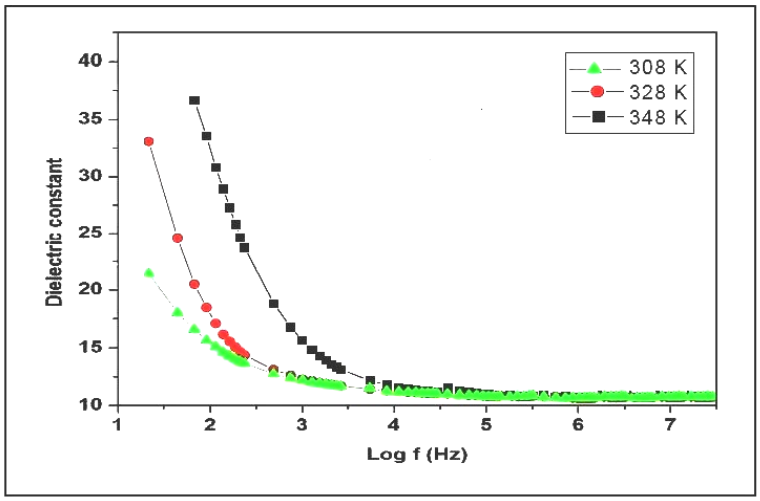

Figure 8. Variation of dielectric constant with log frequency.

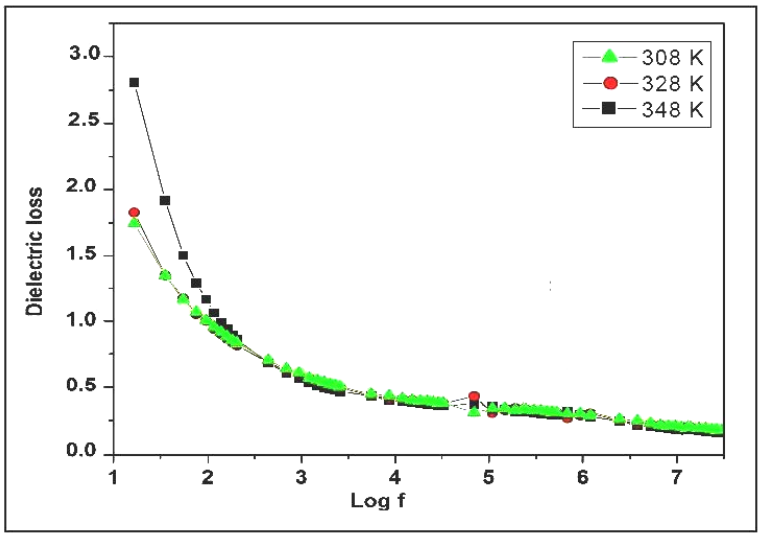

Figure 9. Variation of dielectric loss with log frequency.

behaves as a parallel plate capacitor. Silver paste was used for making the electrode plates on these surfaces of the crystal. The plots of dielectric constant and dielectric loss with frequency for various temperatures are shown in Figures 8 and 9. The dielectric constant is high in the lower frequency region and variation of dielectric constant with log f decreases with an increase in frequency. The high value of dielectric constant at low frequency may be due to presence of all polarizations and its low value at higher frequencies may be due to the significant loss of all polarizations gradually (Sagadevan, 2014). The dielectric loss was also studied as a function of frequency for different temperatures and is shown in Figure 9. The low dielectric loss at high frequencies for the given sample indicates very high purity of the material. This parameter is of vital importance for nonlinear optical materials in their applications. These curves suggest that the dielectric loss is strongly dependent on the frequency of the applied field. The higher values of dielectric loss at low frequencies originate from space charge polarization mechanism and the characteristic of low dielectric loss at high frequencies reveals that the grown crystal possesses relatively high optical quality with low defect density. The behaviour of low dielectric loss with high frequency for the crystal suggests that the crystal possess enhanced optical quality with lesser defects and this parameter plays a vital role for the fabrication of nonlinear optical devices (Suresh and Arivuoli, 2011;

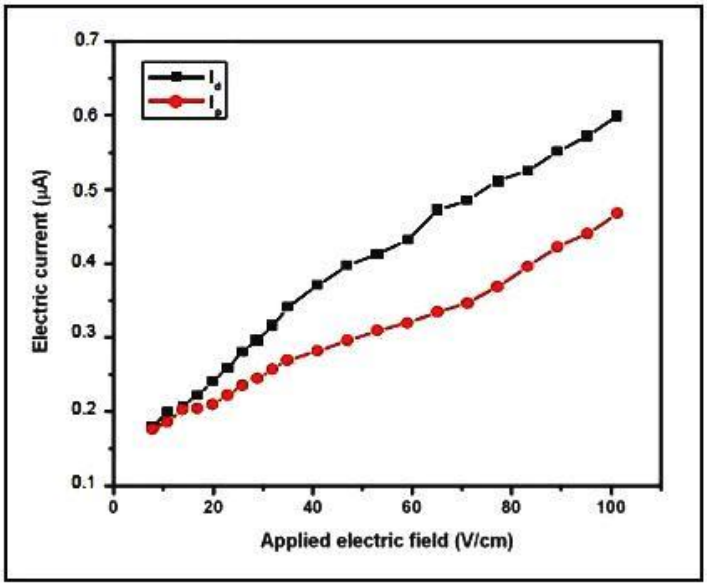

Figure 10. Field dependent photoconductivity of γ- glycine single crystal.

Suresh and Jayaraman, 2011; Balamurugaraj et al., 2013).

Photoconductivity studies

The crystal is well-polished and surfaces are cleaned with acetone. This is attached to a microscope slide and two electrodes of thin copper wire (0.14 cm diameter) are fixed onto the specimen at some distance apart using silver paint. After this, it is annealed at a temperature of 100°C to perfect dryness. A D.C. power supply, a Keithley 485 picoammeter and the prepared crystal was connected in series. The crystal is covered with a black cloth to avoid exposure to any radiation. The current (dark) is measured. To measure the photoconductivity, light from a 100 W halogen lamp is focused onto the crystal. The dark current was recorded by keeping the sample unexposed to any radiation. The Figure 10 shows the variation of both dark current (I_d) and photocurrent (I_p) with the applied electrical field. It is seen from the plots that both I_d and I_p of the sample increase linearly with the applied electrical field.

According to Stockmann model, the forbidden band gap contains two types of centres with energies E_1 and E_2. One type is located between the Fermi level and the conduction band, while the other is situated close to the valence band or between the Fermi level and the valence band. It is also assumed that the first type of centres have a high capture cross section for electrons and the probability of electrons being ejected to the conduction band is very low. In short, the function of these types of centers in the presence of radiation is to create holes (by accepting electrons from the valence band) but at the same time not to increase the number of free electrons. The second type of centres has a high cross-section for electrons and holes and consequently they capture electrons from the conduction band and holes from the valence band and recombine them. Thus, the net number of mobile charge carriers is reduced due to incident radiation giving rise to negative photoconductivity. It is observed from the plot that the dark current is always greater than the photo current, thus confirming the negative photoconductivity (Suresh, 2014).

Conclusion

A single crystal of γ-glycine has been grown by slow evaporation method. The lattice parameters of the grown crystals were determined by single crystal XRD. The different functional groups in the γ- glycine crystal were identified by FTIR spectral analysis. The UV cut-off of γ-glycine crystal is found to be 315 nm. Optical constants such as band gap, refractive index, extinction coefficient and electric susceptibility were calculated from UV-Visible spectrum. TG and DTA reveals that the γ-glycine single crystals are stable upto 305°C. The NLO property of the crystal was examined by performing Kurtz powder test using Nd: YAG laser. The SHG efficiency is found to be 1.5 times than that of KDP. The dielectric constant and dielectric loss of the γ-glycine crystal were calculated for different frequencies and temperatures. The low value of dielectric constant at high frequencies is important for the

device applications. The photoconductivity studies confirm that γ-glycine crystal has negative photoconductivity nature.

Conflict of Interest

The authors have not declared any conflict of interest.

REFERENCES

Prasad PN, Williams DJ (1991). Introduction to Non Linear Optical Effect in Molecules and Polymers, John Wiley & Sons, New York.

Chemla DS, Zyss J (Eds) (1987). Non-linear Optical Properties of Organic Molecules and Crystals, Academic press, New York.

Sagadevan S (2014). Growth, optical and electrical studies of the nonlinear optical crystal: Glycine thiourea. Optik – Int. J. Light Electron. Optics 125(3):950-953.

Sagadevan S (2014). Studies on the optical and dielectric properties of a zinc thiourea chloride NLO single crystal. Optik – Int. J. Light Electron. Optics 125(3):1223-1226.

Suresh S, Arivuoli D (2011). Growth, Theoretical, Optical and Dielectric Properties of L Tartaric Acid NLO Single Crystals. J. Optoelectron.Biomed. Mater.3:63-68.

Koteeswari P, Sagadevan S (2014).Synthesis, growth, and characterization of bisglycine hydrobromide single crystal. J. Mater. 362678:7.

Suresh S, Anand K (2012). Studies on optical, dielectric and electrical conductivity properties of zinc succinate NLO single crystal. Adv. Appl. Sci. Res. 3(2):815-820.

Sagadevan S (2014) Growth, optical, mechanical and electrical studies of nonlinear optical single crystal: Potassium para-nitrophenolate dihydrate. Science Postprint 1(1): e00026.

Sagadevan S, Murugasen P (2014) Studies on Optical, Mechanical and Electrical Properties of Organic Nonlinear Optical p-Toluidine p-Toluenesulfonate Single Crystal. J. Crystallization Process Technol. 4:99-110.

Sagadevan S (2014). Studies on optical, mechanical, dielectric properties of bisthiourea nickel bromide NLO single crystal, Optik - Int. J. Light Electron Opt. 125:6746-6750.

Suresh S, Arivuoli D (2011). Growth, Optical, Mechanical and Dielectric Properties of Glycine Zinc Chloride NLO Single Crystals. J. Minerals Mater. Characterization Eng. 10(12):1131-1139.

Suresh S, Ramanand A, Jayaraman D (2011). Growth, Optical, Dielectric and Fundamental Properties of L-Arginine Acetate NLO Single Crystals. Recent Res. Sci. Technol. 3(1):25-28.

Balamurugaraj P, Suresh S, Mani P, Koteeswari P (2013). Growth, Optical, Mechanical, Dielectric and Photoconductivity Properties of L-Proline Succinate NLO Single Crystal. J. Mater. Phys. Chem. 1(1):4-8.

Suresh S (2014). Investigations on electrical properties of glycine magnesium chloride single crystal. Int. J. Chem. Tech. Res. 6(5):2645-2648.

academicJournals

Vol. 10(13), pp. 430-439, 15 July, 2015
DOI: 10.5897/SRE2015.6269
Article Number:6BEE28154036
ISSN 1992-2248

http://www.academicjournals.org/SRE

Scientific Research and Essays

Full Length Research Paper

Investigation of premature fracture of a tail pulley in the field

J. A. Martins[1]*, I. Kövesdy[2], E. C. Romão[3] and I. Ferreira[1]

[1]State University of Campinas, Materials Engineering Department, UNICAMP, Cidade Universitária 13083-970-Campinas, SP -Brazil.
[2]Metso Minerals, Av. Independência 2500, Bairro Iporanga, Sorocaba, SP Brazil.
[3]Department of Basic and Environmental Sciences, EEL-USP, University of São Paulo, Lorena/SP, Brazil.

Received 28 May, 2015; Accepted 12 June, 2015

An unexpected (premature) failure happened in Tail Pulley during operation in field. Consequently, a complete analysis in terms of fracture and fatigue performed. The analysis aimed to determine the failure root-cause by the analysis of the project and materials. The analysis covered the tensions undergone by the pulleys under operation and the material´s mechanical strengths. The results showed the project conforms the classical mechanics calculations. The failure, on the other hand, characterized as ductile fracture – Fatigue - with crack propagating along 45° referencing the cylinder longitudinal axis. The crack initiated at a flaw found at the weldment region, which resulted a shorter lifetime (collapsing). The sharpen flaw generated a shortcut in the failure process and jumped it straight to the phase of fracture - Stage II fatigue – called crack propagation.

Key words: Tag pulley, stress raiser, critical stress, fatigue.

INTRODUCTION

Mechanical failure of components is always detrimental to equipments and machines and sometimes catastrophic. In the mining or quarry segments failures bring huge prejudices to companies due to downtime (sometimes production impossibility) and costs involved in corrective maintenances. Pulleys are essential to support and allow the conveying of materials and minerals back and forth in the production. Therefore their failures generate always long stoppage in production. A deep analysis of the failed part is notoriously important to preventively avoid recurrence of such event. In this context, the design reanalysis and a “practice x theory” approach when covering wide aspects involved in the failure are mandatory to investigate its real root cause. According to Martins et al. (2009) and Dieter (1986), materials under dynamic cycling are sensitive to stresses state; consequently during the field analysis any flaw in the design or part may be neglected.

According to information’s obtained in field the tail pulley collapsed abruptly and during operation (sees its positioning on the conveyor - Figure 1). The characteristics of the pulley application are; belt conveyor - belt width 762 mm, tensions T_1 and T_2 185 kN and wrapping angle of 180° on the pulley cylinder. The pulley

*Corresponding author. E-mail: jairophd@ig.com.br

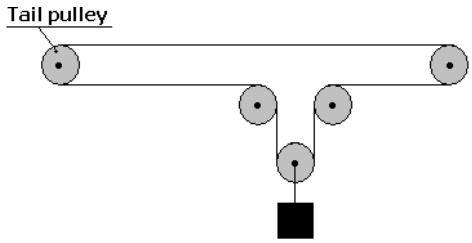

Figure 1. Sketch of conveyor - positioning of the tail pulley.

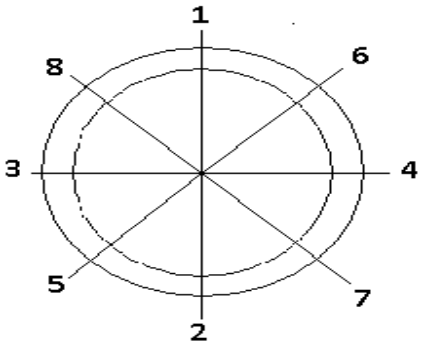

Figure 2. Pulley failed surface mapping.

has an outside diameter of 500 mm, body length (cylinder) 860 mm, and distance between the bearing blocks 1200 mm, shaft diameter at the bearing blocks of 100 mm. The expansion ring used in order to fix and lock the shaft to the pulley hub (its body) was Ring-Feder model 7012, internal diameter 110 mm. This paper aims to analyse the pulley in terms of design, material application and manufacturing, determining the root cause of its abrupt collapse during operation. The study covers the design re-evaluation, the material chemical, metallographic and mechanical property analysis, and the failed surface mapping.

METHODS

Project analyze

The previous calculations done in the design phase were traceable and re-analyzed against the belt conveyor tensions, the material used in the project and the stresses obtained for each component in the assembling. The safety factors identified and compared with the materials mechanical strength and fatigue strength. The residual stresses generated by the welding were not taken into account once the pulley undergoes stress relieve treatment after the manufacturing process. The equations used to evaluate the design of the pulley are those belonged to the classical mechanical equations.

Metallographic analysis, chemical composition and hardness

The chemical and metallographic analysis of the materials of the cylinder and disc succeed in agreement with standards. The purpose was to verify the conformity of both materials with the standard ASTM A-36. The methods to this verification were the electronic microscopy, metallography with etching by Nital 3%, and the Energy Dispersive X-Ray Spectroscopy (EDS) in order to quantify the steel chemical components. The hardness measured in Brinell hardness scale and in a region 200 mm far from the weldment zones.

Mapping the failed surface

Priory of analyzing the failed surface of the cylinder it was cleaned up with the appropriated chemical product (Hydrodesulfurized Heavy). The impregnated particles on the fractured surface were brushed-removed by hand with a steel cord brush. The surface was mapped along 360° and the regions of failure examined microscopically by naked eye. The mapping of the fractured surface followed the sketch at the Figure 2. Pictures were taken from the failure surface (for each region), prioritizing those regions which presented the lesser plastic deformed condition and damages.

Beyond the procedure described, the cylinder sheet was analyzed in terms of quality of weldment. A sample was taken from the cylinder by cutting, grinding and polishing it and then etching with Nital. The intention was to verify the presence of any flaw along the weldment length or cross section. Flaws like discontinuities, voids or cracks, which could lead to failure.

Fracture toughness and fatigue

The component discontinuity dimensions serve as inputs to determine its damage to the component in usage (under load). The mathematical modeling considers the stress intensity for a partial-through thickness flaw, which is given by Dieter (1986), Rabinowicz et al. (2008) and Paris and Erdogan (1963), like follows:

$$\sigma = \frac{KI_c}{\sqrt{\pi \cdot a \cdot \sec\left(\frac{\pi \cdot a}{2t}\right)}} \quad (1)$$

As a rule, whether the critical stress level (σ), in order to make the detected flaw to propagate to failure is lower than the applied stress (σ_a) - in other words (σ_a) is not reached, the flaw won´t propagate as a brittle failure, as follow:

- $\sigma > \sigma_a$ = the crack won´t propagates to failure;
- $\sigma \leq \sigma_a$ = stable, it will propagate to failure.

It is usual in engineering context to place fatigue crack propagation versus the crack length versus cycles at a series of different stress levels, expressed by a general plot of *da/dN* versus ΔK (NASA (1990) and Beden et al. (2009) and Reed et al.(1973). Equation (2) is the appropriate integration to this case. The critical crack length, a_f, at which catastrophic failure can occur (life termination) can be calculated from the following equation:

$$N_f = \frac{1}{A \cdot \sigma_r^p \cdot \pi^{\frac{p}{2}}} \int_{a_i}^{a_f} \alpha(a)^{-p} \cdot a^{-\frac{p}{2}} \cdot da \quad (2)$$

The equation above is due the Stage II of crack propagation and occurs by a plastic blunting process. At the start of the loading cycle the crack tip is sharp, as the tensile load is applied the small double notch at the crack tip concentrates the slip along planes 45° to the

Table 1. Design considerations and results.

Piece	Equivalent stress (MPa)	Material	Yield stress (MPa)	Fatigue limit (MPa)	Ultimate stress (MPa)	Safety factor
Shaft	21	SAE-1045	406	230	675	11
Disc	56	ASTM A36	248	149	400	2,6
Cylinder	26	ASTM A36	248	149	400	9,5

Table 2. Chemical composition, steel ASTM A-36.

ASTM A-36			
Elements	**Standard A-36**	**Cylinder**	**Disc**
%C	0.26 max	0.13	0.13
%Mn	0.6-1.25*	0.71	1.14
P	0.04 max	0.015	0.015
S	0.05 max	0.01	0.01
Si	0.4 max	0.2	0.22
Ni	n/a	0.03	0.03
Cr	n/a	0.005	0
Mo	n/a	0	0
Cu	n/a	0	0
V	n/a	0	0
N	n/a	0.03	0.0067
Al	n/a	0.017	0.022

*Maximum according to standard.

plane of the crack.

RESULTS AND DISCUSSION

Project analyze

After the re-analysis of the design, the calculations are correct and appropriate to the application; the materials properties based on Standard and fatigue limits based on classical technical literature (Beden et al., 2009; Ullman, 1992; Pahl and Wolfgang, 2013). The shaft of the pulley under load presents low stress and deflection, when calculated by Finite Element Method (FEM). The other components, discs and the cylinder are also under low stress levels and appropriate to the application. All stresses respect the safety factors defined previously by the manufacturer based on the project procedures, dictated by the company technology (Table 1).

Metallographic analysis, chemical composition and hardness

The elements quantity in weight and chemical composition are in the Table 2. The material chemical analysis revealed that the materials conforms the standard ASTM A-36. The elements Ni, Cr, Mo, Cu, V, N and Al, as known, are considered residuals into the material, and do not jeopardize its metallurgical or mechanical functions in the application. Figure 3 presents the microstructure of the material A-36 used in the cylinder. Figure 4 presents the same material but now of the discs.

Both, cylinder and disc, present the specified and expected microstructure ferrite and perlite and in accordance with ASTM A36 (Ashby and Cebon, 1993; Metso specification, 1998; Roberts et al., 1988). Any segregation, unexpected microstructure nor cracking were found. The expected hardness at the discs and cylinder are within the specification tolerance. The discs hardness was 135 HB while the cylinder 133 HB, both conform the material hardness specification.

Mapping the failed surface

Figure 5 presents an overview of the mapping of the fractured surface of the pulley, while Figure 6 the two broken parts of the pulley rearranged for a better visualization. Figure 7 just ahead shows only one of the shorter pulley failed piece also for a better comprehension.

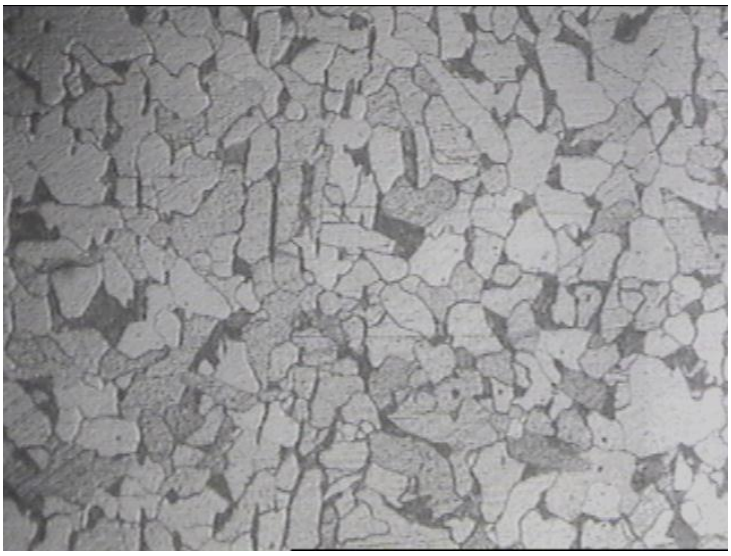

Figure 3. Cylinder - microstructure ferrite and perlite [250X] (Hardness 133 HB) (Specification 119-159 HB).

Figure 4. Disc-microstructure ferrite perlite [250X] (Hardness 135 HB) (Specification 119-159 HB).

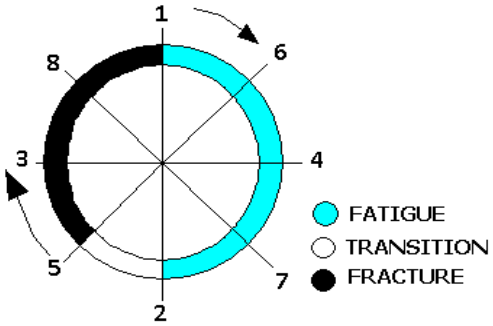

Figure 5. Failure mapping, based on Figure 1.

Figure 6. Pulley overview.

Figure 7. One side of the pulley.

From the Figures 6 to 8 seen that the fracture is macroscopically characterized - by naked eye- as ductile fracture due the crack path (crack propagation, phase II) around 45° (Dieter, 2008). The graph in the Figure 7 maps the height of the fractured cylinder measured from the cylinder face, versus its angular position, separating the different zones along the circulararea. As seen the maximum height of the cylinder was 292 mm to an angular position of 180° (Figure 8).

Failure analysts usually investigate the fracture path to determine the fracture initiation and termination sites, as well as other fractography features. Based on this information, the analyst can also identify various types of monotonic (single cycle) overload, fatigue (multiple cycle) cracking, and time-dependent (creep or corrosion) failure, or combinations thereof (Michael et al., 2007; Richard,

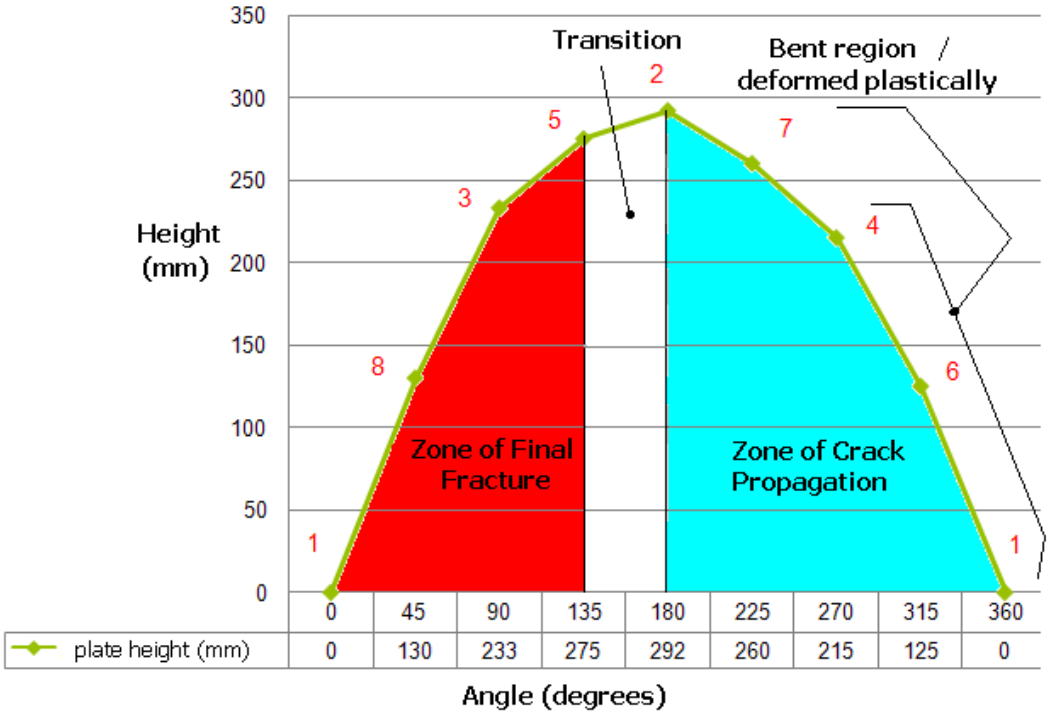

Figure 8. Cylinder plate height.

Figure 9. Zone of crack propagation, point 1, failure initiation and crack propagation.

2011). Figures 9 to 11 aims to reveal the aspects of each of the mapping zones identified in the chart of the Figures 5 and 8.

After a detailed investigation at the failure initiation region and taking a small sample from the cylinder to analyze, one discontinuity found in the zone of crack propagation and particularly close to the crack starting point, at the cylinder longitudinal weldment, more precisely at the interface between disc and cylinder (Figures 12 and 13).

Fracture toughness and fatigue

Figure 14 reveals that the crack dimension despite of being large when compared with the cylinder thickness

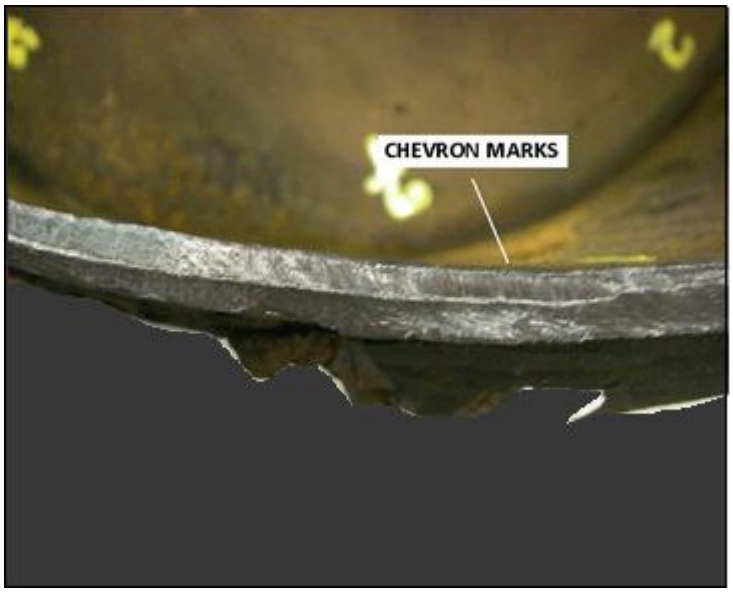

Figure 10. Zone of crack propagation, point 7.

Figure 11. Zone of final fracture, point 8.

(Figure 13), a = 2.5 mm, c = 100 mm against t = 6.35 mm (cylinder thickness), it does not lead to the final fracture, particularly for brittle fracture. The compilation of high material fracture toughness value (K_{Ic}), big crack size and low stress on the cylinder, based on Equation 1 and Table 1, shows the impossibility of brittle fracture. Therefore, the yielding starts a process of slipping planes at the discontinuity, pre-requisite for the Stage I of structural fatigue, called Crack Initiation.

With the fatigue Stage I established due to the pre-existing flaw, it is right to expect a substantial decrease in the lifetime of the pulley under fatigue. As already well established in the literature, this initial fatigue stage theoretically consumes around 80% of the total lifetime of the component to fracture (Figures 10 and 11). Soon after this stage, the crack growths, stage II, and the crack moves instantaneously and fast – consuming the remaining 20% of the total lifetime. The calculated crack growth based on Equation (2) and traced on Figure 15, describes the component (cylinder-pulley) lifetime versus the initial crack size. As described, the low stress at the cylinder, the large crack size and the high $K_I c$ value contribute detrimentally to the cylinder failure. It makes the failing to jump for the crack growth, stage II, which

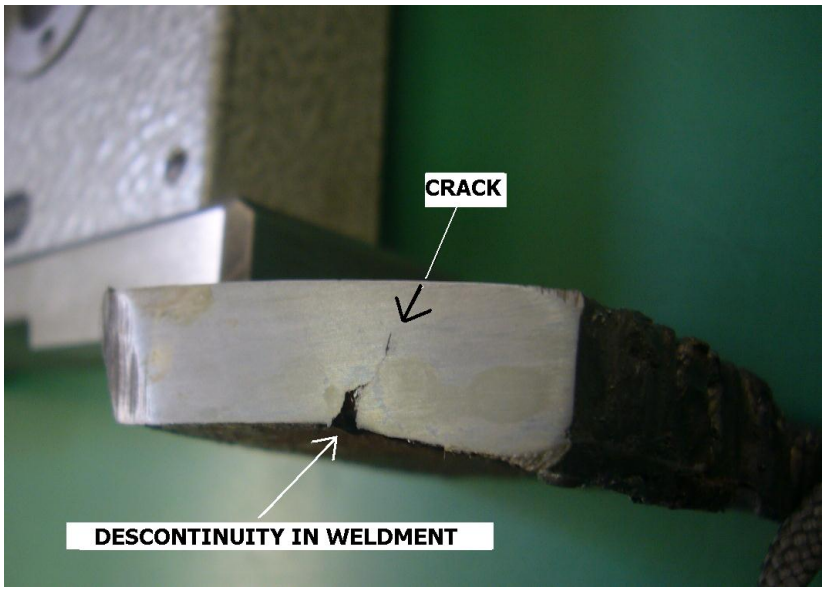

Figure 12. Discontinuity in weldment (a = 2.5 mm).

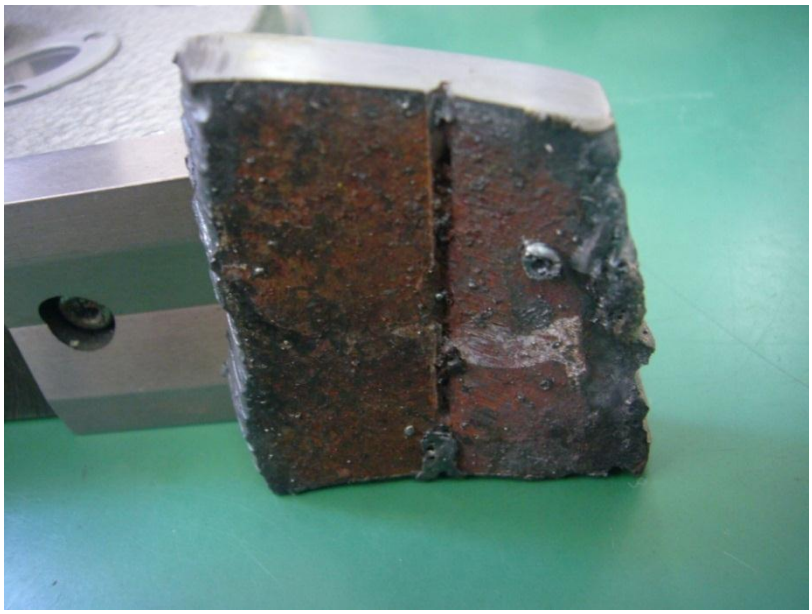

Figure 13. Discontinuity in weldment (a = 2.5 mm; 2c = 100 mm).

speeds up the failure process. The same figure makes clear that flaw (considered stress raisers) with dimension equal of 3.0 mm theoretically results in a lifetime of 10 months. For flaws equal or bigger than 6.0 mm these will not support the application. It means, when loaded into the conveyor the component fails whether just starts being cyclically loaded.

The customer traceability record demonstrates the pulley real lifetime under application in the field as 09 months, pretty close to the theory applied in the analysis.

Conclusions

1. The pulley design is according to the allowable stresses and based on the materials properties;
2. The materials conform with the characteristics in the standard and specification; chemical composition, microstructure and mechanical property (hardness);
3. The failure is not characterized as brittle fracture;
4. Due to the stress raiser (flaws in the weldment zone) the material yield at the crack tip and speed up the

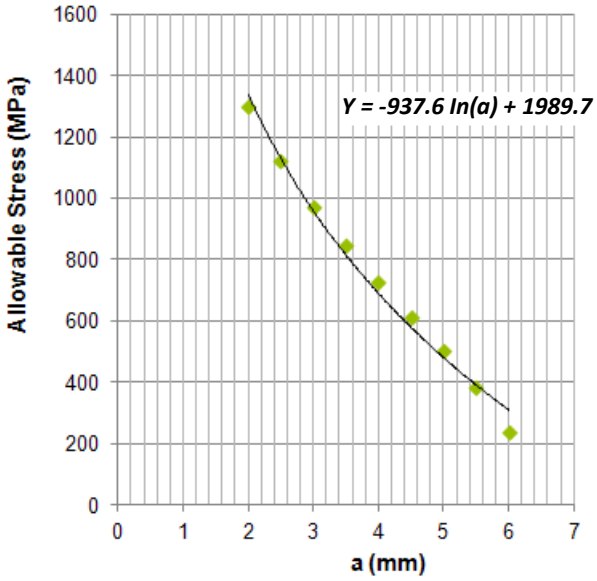

Figure 14. Allowable stress versus crack size.

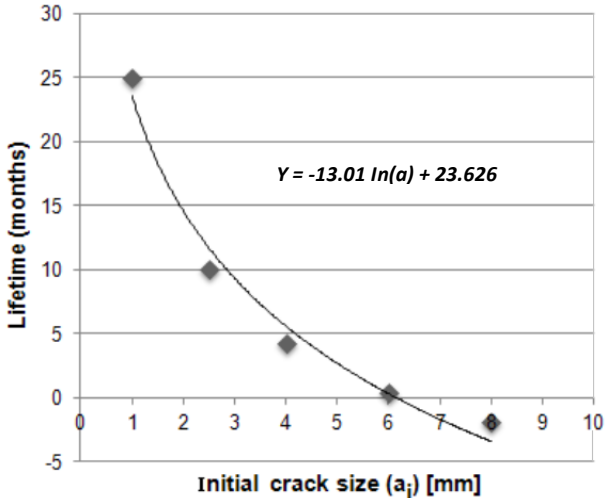

Figure 15. Pulley lifetime versus crack size.

fatigue process. Being the Stage I already accomplished due the flaw presence the fatigue phenomenon jumped straight to the Stage II, crack propagation;

5. Failure micromechanics of chevrons and beach marks found at the failure surfaces reinforce the fatigue presence;

6. The fatigue is characterized as ductile and under low stresses, once the Stage II extends till 180° of the fractured surface;

7. The crack started at the weldment intersection between the disc and cylinder, at the sharpen flaw in the cylinder;

8. The final facture consumed 180° of the fractured surface;

9. The discontinuity presented in the weldment region was the root cause to the fatigue;

10. Comparing the calculated lifetime with the real pulley running in field both are quite similar (calculated - 10 months x real - 09 months).

It is highly recommendable for pulleys but also for all mechanical parts under cyclic loading to have a detailed manufacturing procedure. This procedure must cover all the processes parameters and follow its monitoring and registration along the manufacturing steps. At this manner a more traceable and reliable product is

accomplished.

Conflict of Interest

The authors have not declared any conflict of interest.

ACKNOWLEDGEMENTS

The National Council of Scientific Development and Technology, CNPq, Brazil, (Proc. 408250/2013-5) and FAPESP (Proc. 2014/06679-8) supported the present work.

REFERENCES

Ashby MF, Cebon D (1993). Materials selection in mechanical design. Le J. de Physique IV 3.C7: C7-1.

Beden SM, Abdullah S, Ariffin, AK (2009). Review of Fatigue Crack Propagation Modelsfor Metallic Components. Eur. J. Sci. Res. ISSN 1450-216X. 28(3):364-397.

Dieter GE (2008). Mechanical MetallurgyHardcover - Apr. 1.

ASTM A36 / A36M - 08 Standard Specification for Carbon Structural Steel.

Martins JA, Kovesdy I, Ferreira I (2009). Fracture analysis of collapsed heavy duty pulley in a long-distance continuous conveyors application. Eng. Fail. Anal. 16:2274-2280.

Metso specification (1998). Material A-36, Chemical and Mechanical Properties.

Michael JM, Griebel AH, Tartaglia JM (2007). Fracture surface analysis. Advanced Materials and Processes.

NASA Technical Memorandum 102646 (1990). A Compendium of Sources of Fracture Toughness and Fatigue Crack Growth Data for Metallic Alloys - Part IV.

Pahl G, Wolfgang B (2013). Engineering design: A systematic approach. Springer Science and Business Media.

Paris PC, Erdogan F (1963). A critical analysis of crack propagation laws. J. Fluids Eng. 85(4):528-533.

Rabinowicz Y, Roman I, Ritov Y (2008). Advanced methodology for assessing distribution characteristics of Paris equation coefficients to improve fatigue life prediction. J. Compilation Blackwell Publishing Ltd. Fatigue Fract. Eng. Mater. Struct. 31:262-269.

Reed H, Robert E, Reza A (1973). Physical metallurgy principles. Fourth Edition. Cengage Learning India.

Richard GB (2011). Shigley's Mechanical Engineering Design. Published by Tata Mcgraw Hill Education.

Roberts AWD, Papaliski R, Harrison A (1988). The friction and tension characteristics on driving drums of conveyor belts." Proceedings, 12th Intl. Power and Bulk Solids Handling Conference, Chicago, USA.

Ullman DG (1992). The mechanical design process. New York: McGraw-Hill. 2.

academicJournals

Related Journals Published by Academic Journals

- International NGO Journal
- International Journal of Peace and Development Studies